Journal of Hazardous Materials 388 (2020) 121734

Contents lists available at ScienceDirect

Journal of Hazardous Materials

journal homepage: www.elsevier.com/locate/jhazmat

Removal and recovery of phosphate and fluoride from water with reusable mesoporous Fe_3O_4@*m*SiO_2@*m*LDH composites as sorbents

Feihu Li*, Jie Jin, Ziyi Shen, Huashun Ji, Meng Yang, Yumeng Yin[1]

Collaborative Innovation Center of Atmospheric Environment and Equipment Technology, Jiangsu Key Laboratory of Atmospheric Environment Monitoring and Pollution Control, School of Environmental Science and Engineering, Nanjing University of Information Science and Technology, 219 Ningliu Road, Nanjing 210044, China

GRAPHICAL ABSTRACT

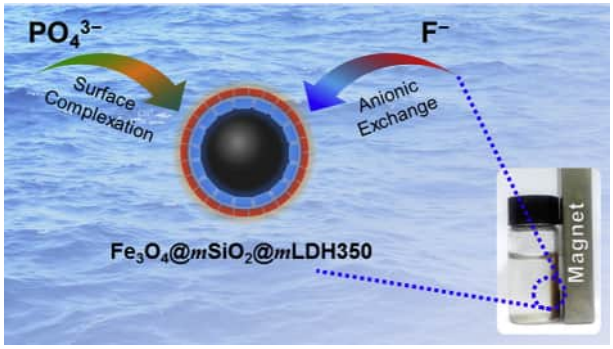

ARTICLE INFO

Editor: G. Lyberatos

Keywords:
Adsorption
Fluoride
Phosphate
Mesoporous
LDHs

ABSTRACT

Three core/shell/shell MgAl-LDH composites using Fe_3O_4 microspheres as the core, a SiO_2 matrix as the inner layer and a MgAl-LDH layer as the outer shell have been synthesized for the removal and recovery of phosphate and fluoride from water by a magnetic separation technique. The synthetic mesoporous MgAl-LDH composites show good magnetic separability, well-defined pore distributions, and have specific surface areas of 73 $m^2 g^{-1}$, 168 $m^2 g^{-1}$, and 137 $m^2 g^{-1}$ for Fe_3O_4@SiO_2@LDH350, Fe_3O_4@SiO_2@*m*LDH350, and Fe_3O_4@*m*SiO_2@*m*LDH350, respectively. The adsorption isotherms of both phosphate and fluoride on these MgAl-LDH composites can be well fitted with the Langmuir model. The maximum adsorption capacities of 57.07 mg g^{-1} and 28.51 mg g^{-1} were obtained on Fe_3O_4@*m*SiO_2@*m*LDH350 for phosphate and fluoride, respectively, much higher than those of other LDH-type materials. The adsorbed phosphate and fluoride could be successfully recovered by $NaNO_3$-NaOH solution, and the regenerated MgAl-LDH composites could be reused for phosphate and fluoride removal. Owing to their high adsorption capacities of both phosphate and fluoride, easy magnetic separation from solution, and good reusability, the mesoporous MgAl-LDH composites are expected to have potential applications in removal or recovery of fluoride or phosphate from water.

* Corresponding author.
E-mail address: fhli@nuist.edu.cn (F. Li).
[1] Present address: Department of Geography and Environmental Science, University of Reading, Reading RG6 6DW, UK.

https://doi.org/10.1016/j.jhazmat.2019.121734
Received 16 September 2019; Received in revised form 19 November 2019; Accepted 20 November 2019
Available online 21 November 2019

1. Introduction

Widespread contamination of aquatic environments, leading to an extensive pollution-induced water shortage and crisis, has been one of the most severe global environmental issues (Eliasson, 2015). Among all water contaminants, phosphorus and fluorine have been recognized as the two most crucial elements in contaminated waterbodies for decades (Ayoob and Gupta, 2006; Sharpley et al., 1994). A continuing elevated level of phosphate in water systems, e.g., lakes, reservoirs, promotes the overwhelming growth of photosynthetic algae and toxic cyanobacteria, resulting in a various extent of eutrophication of standing water bodies (Correll, 1998). For example, the cyanobacterial blooming of Taihu Lake (Eastern China) in the summer of 2007 has caused an enormous and abominable water crisis to the nearby cities (Li et al., 2016). Excessive levels of fluoride in groundwater can also cause plenty of problems for both aquatic organisms and human health (Camargo, 2003). Therefore, the maximum contaminant level (MCL) of fluoride in drinking water is 1.0 mg L^{-1} in China and 1.5 mg L^{-1} according to the World Health Organization (WHO).

To date, a wide variety of technologies have been developed for the removal and recovery of phosphorus and fluoride from water as summarized in many reviews (Bhatnagar et al., 2011; Goh et al., 2008; Loganathan et al., 2014; Morse et al., 1998). Adsorption has received much attention for removing of both phosphate and fluoride anions due to its cost-effectiveness, versatility, operational simplicity, and easy handling of exhausted sorbents (Bhatnagar et al., 2011; Loganathan et al., 2014). Sorbents play a determinative role in adsorptive removal of soluble pollutants including phosphate and fluoride. Among the widespread used sorbents, layered double hydroxides (LDHs) that represent a large family of lamellar inorganic anion exchangers have been extensively investigated for enhanced removal of phosphate and fluoride anions from water because of their ease of preparation, high efficiency, and good performance of reusability (Goh et al., 2008; Cai et al., 2012; Cheng et al., 2010; Chubar et al., 2017; Jia et al., 2018; Lv et al., 2006; Seftel et al., 2018; Wang et al., 2007; Yan et al., 2018). For instance, the fluoride adsorption properties of both pristine and calcined Mg-Al LDHs have been studied for defluorination of drinking water (Cai et al., 2012; Lv et al., 2006; Wang et al., 2007). Phosphate has also shown a strong affinity and hence preferable adsorption onto a series of LDHs (Cai et al., 2012; Cheng et al., 2010; Jia et al., 2018; Seftel et al., 2018; Yan et al., 2018). The adsorption efficiency is a key parameter of LDHs. Various structural modifications of LDHs including calcination (Cheng et al., 2010; Chubar et al., 2017; Wang et al., 2007), doping with other elements (Chubar et al., 2017; Jia et al., 2018; Chitrakar et al., 2007), hybridizations with other composites (Yan et al., 2018; Cai et al., 2016) were extensively used to improve the adsorption performance of either fluoride or phosphate on LDHs.

However, because of the lamellar structure and fine particulate characteristics of LDHs, it's hard to achieve a high-efficient solid-solution separation after the adsorption runs, leading to an unsatisfied recycling performance for adsorptive removal of phosphate and fluoride (Ding et al., 2017; Yan et al., 2015). To address this issue, magnetite (Fe_3O_4) nanoparticles (NPs) were often employed as the magnetic core for the preparation of core/shell Fe_3O_4@LDHs composites for the removal of aqueous pollutants with a highly efficient magnetic separation property. Using Fe_3O_4@SiO_2@AlOOH microspheres as precursors, Shao et al. (2012) prepared a series of core/shell/shell Fe_3O_4@SiO_2@NiAl-LDH microspheres via an *in situ* growth method. The synthetic core/shell microspheres have shown great performance in magnetic separation of histidine-tagged protein. Zhang et al. (2013) also reported a similar core/shell/shell Fe_3O_4@C@NiAl-LDH composite which exhibited high efficiency in the extraction of uranium(VI) ions from aqueous solutions. It has also shown that Fe_3O_4@LDHs composites have fast adsorption kinetics for phosphate removal from water. Recently, (Ding et al., 2017) indicated that the core/shell/shell Fe_3O_4@SiO_2@$m$$CeO_2$ nanocomposite with a mesoporous CeO_2 outermost shell has a high adsorption capacity of phosphate as well as a fast adsorption rate because of the presence of many accessible mesopores. Mandel and coworkers found that Fe_3O_4@SiO_2@Zr-doped LDH exhibited improved phosphate adsorption with great reusability and further demonstrated the feasibility of upscaling the phosphate recovery experiment to a pilot-scale application (Mandel et al., 2013; Drenkova-Tuhtan et al., 2013, 2017). Moreover, our earlier study has demonstrated that mesoporous MgAl-LDHs (denoted as meso-LDHs) can be facilely prepared via a soft-template coprecipitation method and that the synthetic meso-LDHs has exhibited enhanced adsorption performance in both adsorption efficiency and kinetics for bromate uptake from water (Ji et al., 2017), confirming the hypothesis that the introduction of mesopores into LDHs can not only improve the adsorption efficiency but also accelerate the adsorption rate.

To further extend this idea, in this study, we propose a facile route of preparation of a magnetite core/mesoporous SiO_2 shell/mesoporous MgAl-LDHs shell composite for removal and/or recovery of either phosphate or fluoride anions from the water. By using a soft-template hydrothermal method, we synthesized a Fe_3O_4 core with a mesoporous SiO_2 shell nanocomposite (denoted as Fe_3O_4@$m$$SiO_2$) which was further employed as the new core for preparation of core/shell/shell composite (denoted as Fe_3O_4@$m$$SiO_2$@$m$LDHs). The outer shell of mesoporous MgAl-LDHs was anchored to the Fe_3O_4@$m$$SiO_2$ by a soft-template coprecipitation method (Ji et al., 2017). A series of core/shell/shell nanocomposites with or without mesoporous shells have also been prepared and evaluated for the adsorption efficiency of phosphate and fluoride uptake from water. Moreover, the recycling performance of these MgAl-LDH composites was also examined to explore its potential as a cost-effective sorbent for removal or recovery of either phosphate or fluoride anions from the water.

2. Experimental section

2.1. Materials

Magnesium nitrate hexahydrate ($Mg(NO_3)_2{\cdot}6H_2O$, ≥ 99%) and aluminum nitrate nonahydrate ($Al(NO_3)_3{\cdot}9H_2O$, ≥ 98%) were purchased from Sinopharm Chemical Reagent Co., Ltd. (Shanghai, China). Pluronic F127 was obtained from Sigma-Aldrich Co. (Shanghai, China). Milli-Q water (18 MΩ-cm, 25 °C) was used to prepare solutions. All other chemicals were of A.R. grade and obtained from Sinopharm Chemical Reagent Co. Ltd. and used as received unless otherwise stated. The phosphate stock solution (1000 mg L^{-1}) was prepared by dissolving a certain amount of KH_2PO_4 (≥ 99%) with ultrapure water. Likewise, the fluoride stock solution (100 mg L^{-1}) was also made by mixing a given amount of NaF (≥ 98%) with ultrapure water and both stock solutions were stored in a lab refrigerator (4 °C) for further use. HNO_3 and NaOH solutions (0.1 M) were used to adjust the pH values of solutions.

2.2. Preparation of Fe_3O_4@$m$$SiO_2$@$m$LDHs composites

Magnetic core/shell/shell mesoporous LDHs composites were prepared stepwise following a method similar to the procedure as reported previously (Shao et al., 2012). The synthesis procedure involves three steps: i) preparation of Fe_3O_4@$m$$SiO_2$ via a soft-template hydrothermal method; ii) preparation of Fe_3O_4@$m$$SiO_2$@$m$LDHs inorganic-organic hybrids via the soft-template coprecipitation approach at 65 °C (Ji et al., 2017); iii) preparation of Fe_3O_4@$m$$SiO_2$@$m$LDH350 composites by calcination at 350 °C (the organic template removal process). The synthesis procedure is illustrated in Scheme 1.

Briefly, uniform magnetite microspheres were prepared following the method as depicted previously by Shao et al.[24] Then 0.1 *g* of Fe_3O_4 microspheres were ultrasonically dispersed into 50 mL HCl (0.1 M) for 10 min and then separated and washed three times with deionized water (DI H_2O). The clean Fe_3O_4 samples were then homogeneously

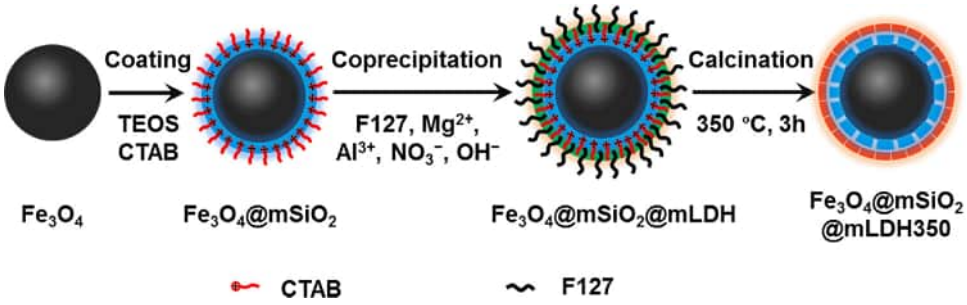

Scheme 1. Schematic illustration of the preparation of Fe_3O_4@*m*SiO_2@*m*LDH350 composite.

dispersed in a solution of ethanol (80 mL), deionized water (20 mL), concentrated ammonia aqueous solution (1.0 mL, 28 wt.%), and cetyltrimethylammonium bromide (CTAB; 0.03 *g*, 0.082 mmol), followed by the addition of tetraethyl orthosilicate (TEOS; 0.03 *g*, 0.144 mmol). After transferring to a sealed Teflon-lined stainless autoclave (100 mL), ageing in a oven at 100 °C for 4 h and air-cooling to room temperature, the off-white precipitate was recovered by centrifuging at 4000 RPM, followed by washing with hot 50% ethanol (v/v) for several times to remove the remaining surfactant. Fe_3O_4@*m*SiO_2 microspheres were obtained by drying in a vacuum at 60 °C for 6 h. For the preparation of magnetic composites with mesoporous LDHs outer shell, 2.4 *g* of F127 was firstly dissolved in 120 mL of deionized water. Then, a mixture of $Mg(NO_3)_2{\cdot}6H_2O$ (12.3 *g*, 48 mmol) and $Al(NO_3)_3{\cdot}9H_2O$ (9.02 *g*, 24 mmol) was added and stirring for 10 min to form a transparent solution. 0.48 *g* of Fe_3O_4@*m*SiO_2 was then added, followed by dropwise addition of an alkaline solution (0.1 mol NaOH and 0.048 mol $NaNO_3$ in 100 mL H_2O) until the pH is about 9.5. The suspension was then aged at 65 °C for 18 h, and the off-white precipitate was recovered by centrifugation, washing with deionized water for several times, and freeze-drying overnight. Finally, the magnetic core-shell mesoporous LDHs composite, Fe_3O_4@*m*SiO_2@*m*LDH350, was obtained by calcination at 350 °C for 3 h and air-cooling to room temperature. For comparison, Fe_3O_4@SiO_2 composites were also prepared following the previous procedure (Shao et al., 2012). Then, using Fe_3O_4@SiO_2 as the new core, other two LDHs composites, Fe_3O_4@SiO_2@LDH350 and Fe_3O_4@SiO_2@*m*LDH350, were also prepared following the above procedures in the absence and presence of F127, respectively.

2.3. Characterizations

Powder X-ray diffraction (XRD) patterns of all mesoporous LDHs composites and Fe_3O_4 were collected using on a Shimadzu XRD-6100 diffractometer with a Cu Kα radiation (λ = 1.54178 Å), a scan step of 0.02° and a scan rate of 5° per minutes. Fourier transform infrared (FTIR) spectra of the LDHs composites before and after adsorption were recorded with a Nicolet iS5 spectrometer (Thermo Fisher, USA) using the KBr-pressed-disc method. The Brunauer-Emmett-Teller (BET) specific surface areas, and the Barrett-Joyner-Halenda (BJH) pore size distributions of the LDHs composites were measured by N_2 adsorption-desorption at −196 °C using a Quantachrome gas adsorption analyzer (iQ-AG-MP). Prior to the measurement, the samples were degassed at 105 °C for at least 6 h. The morphological structures were investigated on a Hitachi SU1510 Scanning Electron Microscope (SEM) at an accelerating voltage of 1.5 kV and a JEOL JEM-2100 F Field Emission Transmission Electron Microscope (FETEM) equipped with an OXFORD Energy Dispersive X-ray Spectrometer (EDX). Zeta (ζ) potential data were collected on a Zetasizer Nano ZS 90 apparatus (Malvern, UK) using 10 mM of $NaNO_3$ solution as the background electrolyte. X-ray photoelectron spectroscopy (XPS) (PHI 5000 Versa Probe, UIVAC-PHI, Japan) with a monochromatized Al Kα X-ray source ($h\nu$ = 1486.6 eV) was employed to evaluate the surface properties of the LDHs composites before and after adsorption. The adventitious C 1*s* peak (284.8 eV) was used for the calibration of the binding energy values of other elements.

2.4. Batch adsorption tests

All batch adsorption experiments were performed at atmospheric pressure and room temperature (*ca*. 25 °C). The adsorption of F^- and PO_4^{3-} on three mesoporous LDHs composites (i.e., Fe_3O_4@SiO_2@LDH350, Fe_3O_4@SiO_2@*m*LDH350, and Fe_3O_4@*m*SiO_2@*m*LDH350) was investigated via three sets of batch experiments – the effects of pH and ionic strength (*IS*), the effects of pH and initial adsorbate concentration (C_0), and adsorption isotherms. The effects of pH and IS on adsorption were examined in polyethylene centrifuge tubes sealed with screw-cap under N_2 condition in the presence of 1 mM, 10 mM, and 100 mM $NaNO_3$ background electrolyte over a range of pH values from 3 to 12. The adsorption slurries were prepared in 10-mL polyethylene centrifuge tubes by mixing 10 mg sorbents with an amount of phosphate or fluoride stock solution and the background electrolyte solution, $NaNO_3$ (1 mM, 10 mM, 100 mM), giving a total volume of 10 mL suspension with a final concentration of 1 *g* L^{-1} of sorbent and 10 mg L^{-1} of adsorbates, respectively. The pH was adjusted with 0.5 M or 0.1 M HNO_3 or NaOH solution. Afterward, the suspensions were bubbled with N_2 for 5 min to exclude dissolved O_2 and CO_2 and equilibrated for 24 h on a Labquake tube rotator (Thermo Scientific, USA) at 60 RPM. Then the solid sorbents and liquid phases were separated by centrifugation at 8000 rpm for 10 min followed by filtration with 45 μm mixed cellulose esters (MCE) membrane (Navigator, Tianjin). The concentrations of PO_4^{3-} and F^- in the supernatant were analyzed using the complexone method and the vanadomolybdophosphoric acid method (Drenkova-Tuhtan et al., 2017). The pH of solutions was measured by using an Orion pH meter (Model 868) calibrated with standard pH 4.00, 6.86 and 9.18 buffers (Leici, Shanghai). Likewise, the effects of pH and C_0 on adsorption were also performed in the presence of 2 mg L^{-1}, 10 mg L^{-1}, and 30 mg L^{-1} adsorbates (PO_4^{3-} or F^-) in a constant background electrolyte (10 mM $NaNO_3$) at different pH values ranging from 3 to 12. The adsorption isotherm experiments were conducted at a pH of 7.5 ± 0.2. The sorbent dosage was fixed at 1 *g*/L, whereas the concentrations of As(V) and F^- were varied in the range of 1–100 mg L^{-1}.

The adsorption percentage (%) and the adsorption capacity (Q, in mg g^{-1}) of sorbents were calculated by the following equations:

$$\text{Adsorption (\%)} = \frac{C_0 - C_e}{C_0} \times 100\% \quad (1)$$

$$Q = \frac{C_0 - C_e}{m} \times V \quad (2)$$

where m is the mass of sorbents (in g), V is the volume of suspension (in mL), C_0 and C_e (in mg L^{-1}) are the initial and the equilibrium concentrations of adsorbates in the suspensions, respectively.

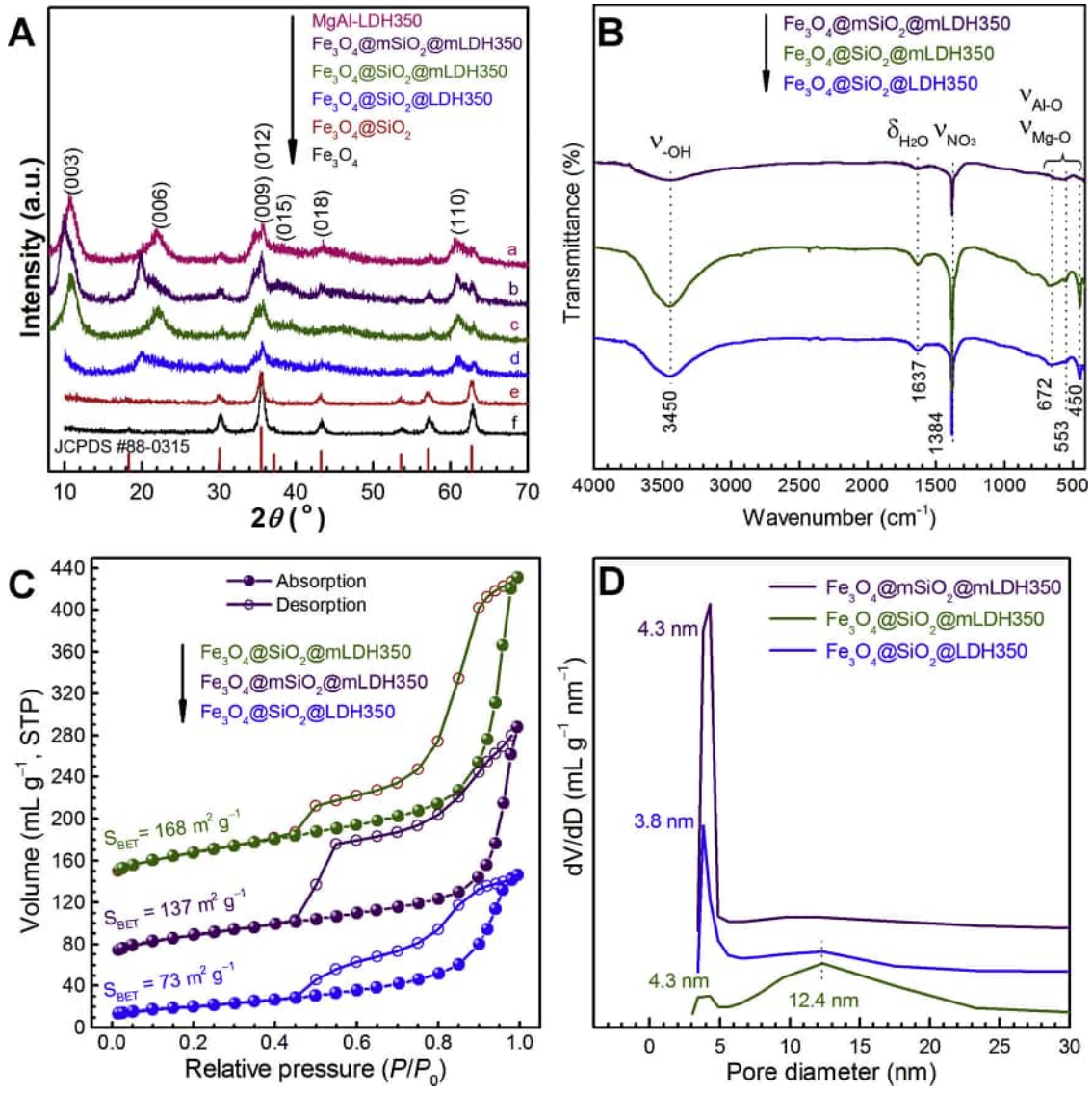

Fig. 1. Characterizations of mesoporous MgAl-LDH composites: (A) XRD patterns; (B) FTIR spectra; (C) N_2 absorption-desorption isotherms at −196 °C; and (D) the corresponding BJH pore size distribution plots.

2.5. Regeneration and reuse tests

Sodium nitrate and sodium hydroxide mixed solutions (10 mM $NaNO_3$ + 100 mM NaOH, 1:1 (v/v)) were used as the regenerant here as in our previous study (Ji et al., 2017). Upon completion of the first cycle adsorption of PO_4^{3-} or F^-, the exhausted sorbent was regained with an external magnet and regenerated by mixing mechanically with the regenerant solution. The sorbent was retrieved by centrifugation, followed by rinsing with ultrapure water three times before the next adsorption cycle. The adsorption-regeneration-reuse tests were performed continuously for five cycles to explore the possibility of reusing the exhausted sorbents. The regeneration efficiency was evaluated by measuring the recovered adsorption capacities for PO_4^{3-} or F^- after regeneration.

3. Results and discussion

3.1. Characterization of Fe_3O_4@mSiO_2@mLDHs composites

Fig. 1A shows the XRD patterns of Fe_3O_4, Fe_3O_4@SiO_2, Fe_3O_4@SiO_2@LDH350, Fe_3O_4@SiO_2@*m*LDH350, Fe_3O_4@*m*SiO_2@*m*LDH350, and MgAl-LDH350. Obviously, the reflections in curve *f* (pure Fe_3O_4) can be well indexed as the magnetite phase (JCPDS #88-0315). These reflections remained after the coating of a SiO_2 layer (curve *e*), but their intensities decrease to some degree due to the SiO_2 coating as previously observed by Shao and his co-workers (Shao et al., 2012). After coating with the MgAl-LDH layer, the reflection intensities of Fe_3O_4 decrease further (blue curve in Fig. S1 in the Supporting information). Meanwhile, a series of well-defined reflections attributable to (003), (006), (009)/(012), (015), (018), and (110) planes of MgAl-LDH rose up, indicating the formation of the outermost MgAl-LDH shell with high crystallinity. After calcination at 350 °C, the reflection intensities decreased evidently but the proportional relationship of these reflections remained (curve *d* in Fig. 1), indicating the formation of a poorly crystallized MgAl-LDH shell. The decrease in reflection intensities has also been observed for other core/shell/shell MgAl-LDH composites after calcination at 350 °C (*cf.* Fig. 1 and S1). It is worth noticing that Fe_3O_4@*m*SiO_2@*m*LDH350 (curve *b*) shows a very similar XRD pattern as Fe_3O_4@SiO_2@*m*LDH350 (curve *c*) — comprising a series of reflections assignable to MgAl-LDHs as well as some typical reflections of magnetite. This observation indicates that both samples have similar phase compositions and that the formation of the outermost MgAl-LDH shell is independent upon the presence of F127 in the precursor mixture during the shell coating stage. The estimated thicknesses of the

outermost LDH shells based on the full width at half maximum (FWHM) of the (003) basal plane are 4.2 nm and 4.0 nm for Fe_3O_4@*m*SiO_2@*m*LDH350 and Fe_3O_4@SiO_2@*m*LDH350, respectively (Gunawan and Xu, 2009). Moreover, the peak intensities of both samples are greater than the corresponding peaks of Fe_3O_4@SiO_2@LDH350, suggesting that the presence of F127 in the precursor mixture probably improves the crystallinity of MgAl-LDH (Ji et al., 2017).

The FTIR spectra of mesoporous MgAl-LDH composites (Fig. 1B) provide evidence for the presence of NO_3^- anions (band at 1384 cm^{-1}) in the interlayer region of MgAl-LDH after calcination at 350 °C. Fig. 1C displays the N_2 absorption-desorption isotherms measured at −196 °C for MgAl-LDH composites. All the samples exhibit a type IV isotherm behavior with a hysteresis loop of type H2 at high relative pressures ($P/P_0 > 0.4$) according to the IUPAC classification, which corresponds to ink-bottle-like mesopores (Ji et al., 2017). These results are further confirmed by the well-developed uniform mesopores at mean values of 4.3 nm and 3.8 nm for Fe_3O_4@*m*SiO_2@*m*LDH350 and Fe_3O_4@SiO_2@*m*LDH350, respectively in the BJH pore size distribution (PSD) plots (Fig. 1D). In the case of Fe_3O_4@SiO_2@LDH350, it shows a broad PSD centered at 12.4 nm along with a narrow mesopore centered at 4.3 nm, both of which are probably derived non-rigid aggregates of plate-like LDH particles (Thommes et al., 2015). Fe_3O_4@SiO_2@LDH350 has a BET specific surface area of 73 $m^2 g^{-1}$, which is close to that of Fe_3O_4@SiO_2@ZnAl-LDH (75 $m^2 g^{-1}$) as reported previously (Shao et al., 2012). The BET specific surface areas are 168 $m^2 g^{-1}$ and 137 $m^2 g^{-1}$ for Fe_3O_4@SiO_2@*m*LDH350 and Fe_3O_4@*m*SiO_2@*m*LDH350 respectively, which are much greater than that of Fe_3O_4@SiO_2@NiAl-LDH microspheres prepared by (Shao et al., 2012), further confirming that the introduction of mesopores by the soft-template method can greatly improve the specific surface areas of LDH composites (Ji et al., 2017).

By use of the SEM image data, particle size distribution analysis was performed with ImageJ (version 1.51) for all samples and the PSD histograms are given as insets in Fig. 2A-B. The SEM image indicates that the Fe_3O_4 microspheres are nearly monodisperse with a mean diameter of ~ 395 nm (Fig. S2A and S2B). To improve the bonding between the outer LDHs shell to the inner Fe_3O_4 core, a SiO_2 layer was generally sandwiched, forming a core/shell/shell hierarchical structure (Shao et al., 2012). After coating a mesoporous SiO_2 layer, the mean diameter of Fe_3O_4@*m*SiO_2 microspheres increased to ~ 469 nm (inset of Fig. 2A, and Fig. S2C), indicating that the thickness of the mesoporous SiO_2 layer is about 74 nm. Further coating of mesoporous MgAl-LDH to the Fe_3O_4@*m*SiO_2 microspheres to the Fe_3O_4@*m*SiO_2 microspheres and calcination at 350 °C led to the formation of core/shell/shell structured Fe_3O_4@*m*SiO_2@*m*LDH350 composite with a mean diameter of ~ 503 nm (inset of Fig. 2B, and Fig. S2D). It's noted that the outmost mesoporous MgAl-LDH layer is very thin (~ 34 nm). This observation is further confirmed by the TEM images as shown in Fig. 2C − D and in good agreement with the previous study (Zhang et al., 2013). In addition, the high angle annular dark field-scanning transmission electron microscopy (HAADF-STEM) image and the corresponding EDX mapping (Fig. 2E-F) verified the co-existence of Fe, O, Si, Mg, and Al elements. It's also observed that iron is located in the center of the single microsphere (Fig. 2E inset), whereas both Mg and Al are well dispersed throughout the whole microsphere. Moreover, The diameter of the single microsphere in terms of its EDX mapping data increased slightly in the order of Fe < O < Si < Al ~ Mg, further confirming the core/shell/shell hierarchical structure of the Fe_3O_4@*m*SiO_2@*m*LDH350 composite.

3.2. Points of zero charge and water dispersion stability

Fig. 3 shows the zeta (ζ) potential plots as a function of pH, phosphate and fluoride anions. In the absence of phosphate or fluoride, the point of zero charge (pH_{PZC}) values of all MgAl-LDH composites as determined by the Zetasizer apparatus were in the range of 8 − 11, in good consistency with those as reported in previous literature (Ji et al., 2017; Huang et al., 2014; Park and Kim, 2011). In the presence of either phosphate or fluoride, the pH_{PZC} values of all MgAl-LDH composites shifted remarkably towards the lower pH value, indicating higher affinity of both phosphate and fluoride anions than nitrate in the interlayer region of MgAl-LDH composites (Cai et al., 2012). This is in good agreement with the affinity order of common intercalated anions, among which the more strongly bound anions are those with the smaller ionic radii (Ulibarri and Hermosin, 2001). The presence of 1 mM of phosphate in the tested suspensions can definitely shift the pH_{PZC} values of Fe_3O_4@SiO_2@LDH350, Fe_3O_4@SiO_2@*m*LDH350, Fe_3O_4@*m*SiO_2@*m*LDH350 from 8.6, 8.8, and 9.0 to 5.9, 4.9, and 4.5, respectively, whereas the existence of 1 mM of fluorides can greatly decrease the above pH_{PZC} values to more acidic range (Fig. 3). This observation can be explained by the fact that fluoride anion has a higher affinity than phosphate species such as $H_2PO_4^-$, and HPO_4^{2-} (Ulibarri and Hermosin, 2001). The strongly bound fluoride would somewhat decrease the spacing between the layers and consequently affect the desorption efficiency of the intercalated anions in the regeneration process.

Generally, the shift of pH_{PZC} to a more acidic range in the presence of the tested adsorbate species can be used as indirect macroscopic evidence of inner-sphere surface complex formation at the water-mineral interface in the cases of anion adsorption on most metal oxides (Goldberg, 2014; Li et al., 2019). However, in the case of LDHs, besides the adsorption of anions by the surface metal hydroxyls (termed as > M–OH) of LDH layers, anionic exchange of the intercalated anions with the anions in solution and reconstruction of the lamellar structure of calcined LDHs (the rehydration process) also account for the uptake of anions from solution (Ji et al., 2017; Delgado et al., 2008).

The water dispersion stability of Fe_3O_4@*m*SiO_2@*m*LDH350 and non-magnetic meso-LDH350 suspensions were also investigated by the free sedimentation method. The results shown in Fig. S3 indicate that the light red Fe_3O_4@*m*SiO_2@*m*LDH350 suspension shows more light adsorbance in the higher wavelength range (λ > 500 nm) as compared to the pale white meso-LDH350 suspension (Fig. S3A), and that the optical transmittance of both suspensions increased apparently with sedimentation time at almost the same slope (Fig. S3B). This observation suggests that both the magnetic and non-magnetic suspensions have a poor water dispersion stability and that the magnetic core in Fe_3O_4@*m*SiO_2@*m*LDH350 plays very little role in improving its dispersion stability.

3.3. Effects of pH and ionic strength

Effects of pH and ionic strength (*I*) on phosphate (PO_4^{3-}) and fluoride (F^-) adsorption on mesoporous MgAl-LDH composites were investigated in detail from pH 3 to 12 at I = 1 mM, 10 mM, and 100 mM $NaNO_3$ solution, respectively. The results were depicted in Fig. 4A and S4. It was found that PO_4^{3-} adsorption efficiencies (Adsorption%) exhibit almost independent upon both pH and ionic strength at pH < pH_{PZC} (i.e., 9.0 for Fe_3O_4@*m*SiO_2@*m*LDH350), indicating that most of the phosphates were bound with surface metal hydroxyls (i.e., > Al − OH and > Mg − OH) via inner-sphere complexation (Goldberg, 2014). This speculation is also validated by the fact that MgAl-LDHs often have a higher affinity toward hydroxyl ions (OH^-) in solution than phosphate species such as $H_2PO_4^-$, and HPO_4^{2-} (Ulibarri and Hermosin, 2001), both of which predominate over other aqueous species of phosphate across a range of pH values from 3 to 9 (Fig. 4C). Above the pH_{PZC}, as I increased from 1 mM to 100 mM $NaNO_3$, the adsorption efficiencies decrease slightly with increasing pH values from 9 to 12 (Fig. 4A). This behavior is probably arisen from the Coulomb repulsion between the negative-charged surfaces of MgAl-LDHs due to the excessive OH^- in solution and the multivalent phosphate anions such as HPO_4^{2-} and PO_4^{3-} (Cai et al., 2012). However, the data of phosphate adsorption on Fe_3O_4@*m*SiO_2@*m*LDH350 are quite different from the two following studies. It has shown that the phosphate

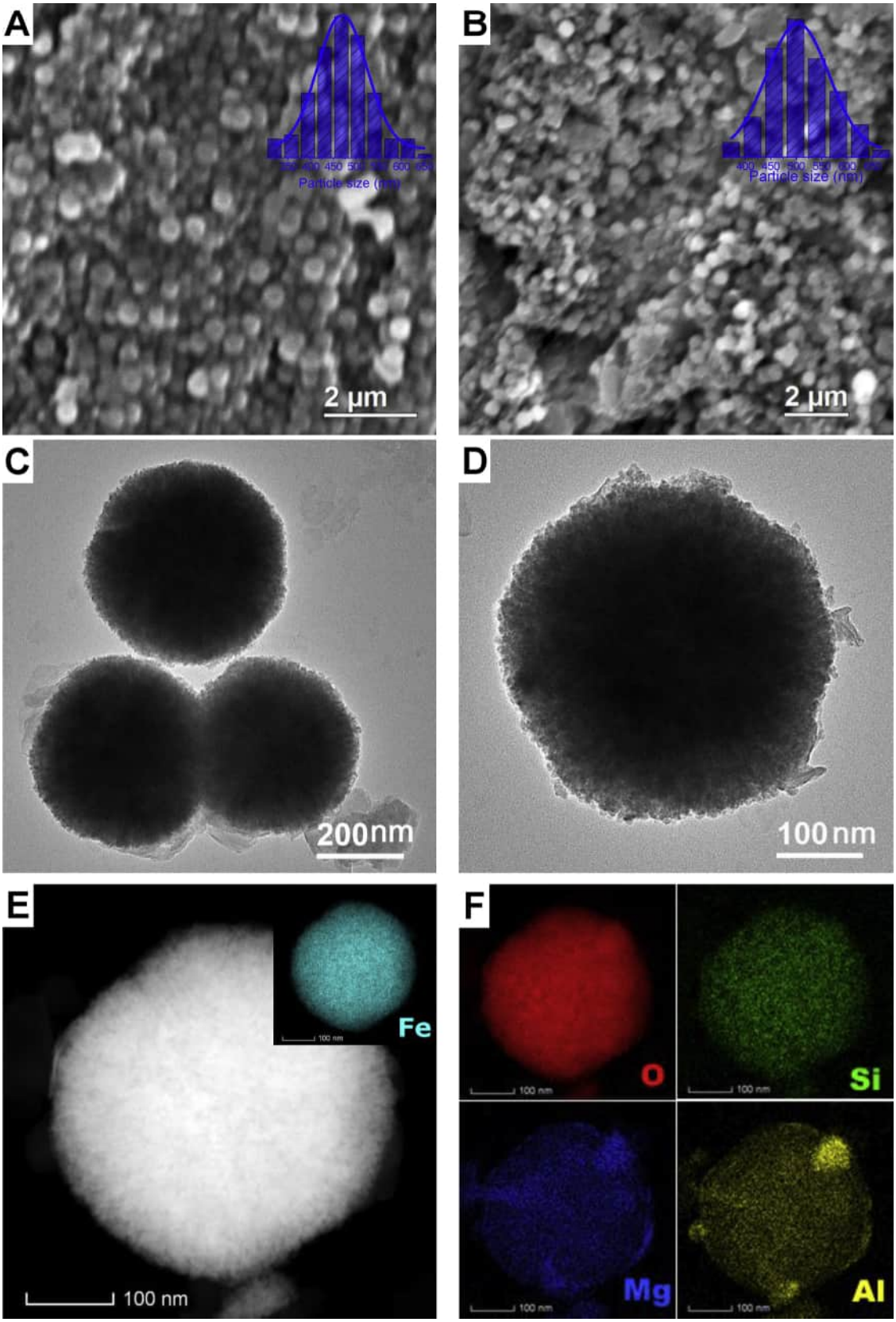

Fig. 2. SEM and TEM images of (A) Fe_3O_4@*m*SiO_2; (B–D) Fe_3O_4@*m*SiO_2@*m*LDH350 microspheres; (E, F) HAADF-STEM image and the corresponding EDX mapping results of a single Fe_3O_4@*m*SiO_2@*m*LDH350 microsphere.

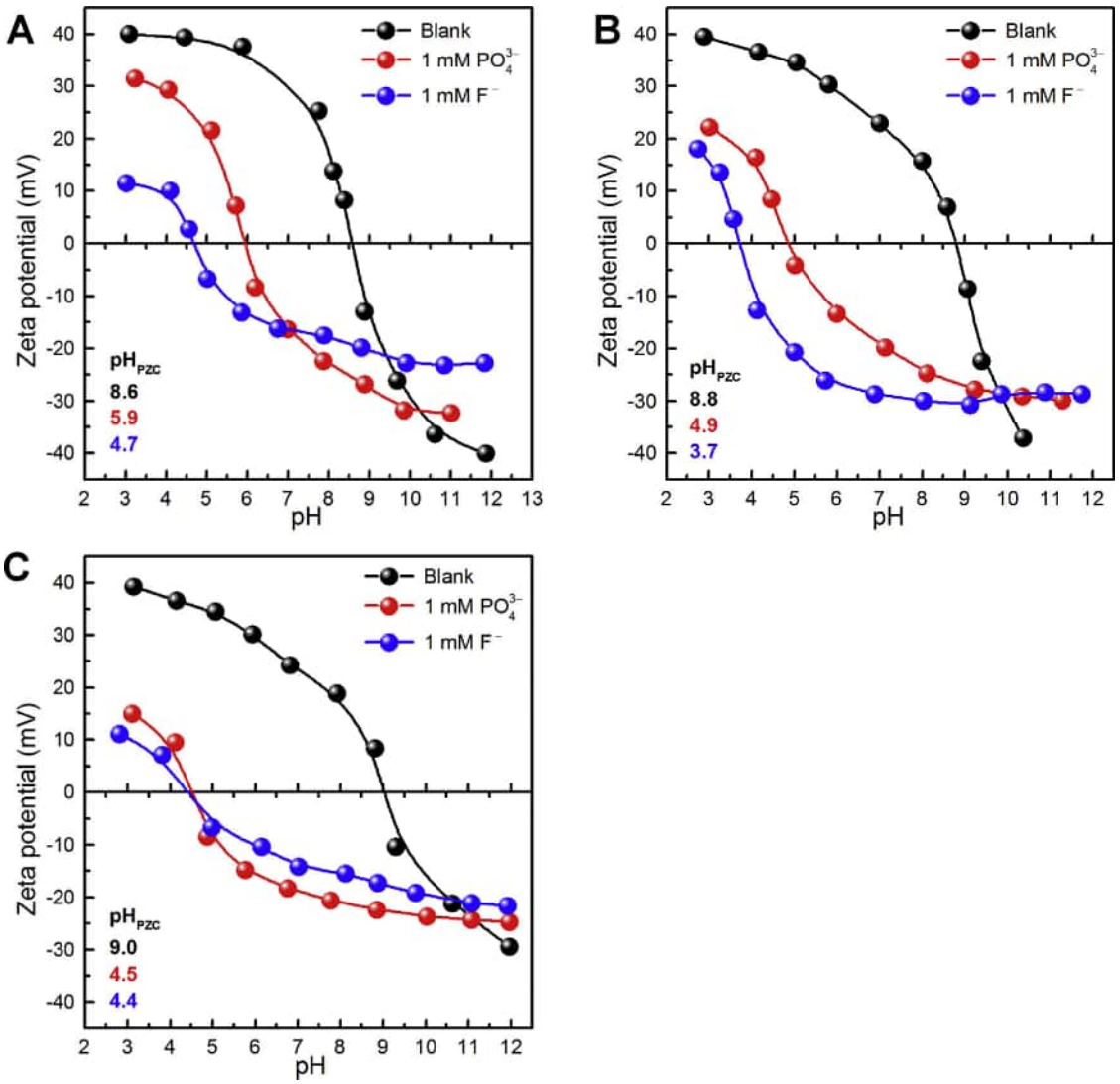

Fig. 3. Zeta (ζ) potential profiles of (A) Fe_3O_4@SiO_2@LDH350, (B) Fe_3O_4@SiO_2@*m*LDH350, (C) Fe_3O_4@*m*SiO_2@*m*LDH350 in the absence or presence of either phosphate or fluoride. (I = 1 mM $NaNO_3$, sorbent dosage = 0.1 g L^{-1}, T = 20 °C).

adsorption efficiencies of MgAl-LDHs (calcined at 500 °C) increased with pH to a maximum at pH 5 and then decreased gradually with pH from 5 to 11 (Das et al., 2006). It was believed that the lower adsorption efficiencies at pH < 5 was due to the partial dissolution of the calcined MgAl-LDHs and that the decrease in adsorption efficiencies at higher pH was derived from the increasing competition from OH^- (Das et al., 2006). It was also observed a similar trend of phosphate adsorption on calcined MgAl-LDHs with CO_3^{2-} as the intercalated anions (Cai et al., 2012). Annealing of MgAl-LDHs at above 500 °C will definitely lead to the collapse of the layered structure and the formation of a mixture of aluminum and magnesium oxides (MgO) that will dissociate in solution with a pH value below 5 (Cai et al., 2012; Das et al., 2006). In our cases, however, it should be stressed that calcination at 350 °C not only allows the survival of the lamellar structure of the outermost MgAl-LDH shells but also improves the formation of mesopores in the shells (Fig. 1) (Ji et al., 2017). The unique features are believed to endow these core/shell/shell mesoporous MgAl-LDH composites with superior adsorption performance of phosphate over the pH range studied.

In contrast to the case of phosphate adsorption, the fluoride adsorption efficiency of Fe_3O_4@*m*SiO_2@*m*LDH350 was strongly influenced by both pH and ionic strength. For example, in the case of I = 1 mM $NaNO_3$, the F^- adsorption efficiencies decreased gradually from 85.3% to 73.5% when pH values increased from 3 to 8.8. This is because of the increased competitive adsorption from excess OH^- ions that are more preferred bound by MgAl-LDHs than F^- anion (Cai et al., 2012; Ulibarri and Hermosin, 2001), which are the predominant species over the range of pH values from 3 to 12 (Fig. 4D). The adsorption efficiencies further declined rapidly with increasing pH values above pH_{PZC} (i.e., 9.0) due to the combined effects of increasing competition from OH^- and the Coulomb repulsion between the negative-charged surfaces of Fe_3O_4@*m*SiO_2@*m*LDH350 and F^- in solution. With the increase of ionic strength from 1 mM to 10 mM and 100 mM $NaNO_3$, the F^- adsorption efficiencies decreased apparently over the pH range studied, implying that F^- was bound mainly by the anionic exchange with the intercalated NO_3^- (Chubar et al., 2017; Wang et al., 2007; Kameda et al., 2017). Furthermore, as shown in Fig. S4, both PO_4^{3-} and F^- adsorption on the other two MgAl-LDH composites (i.e., Fe_3O_4@SiO_2@LDH350, and Fe_3O_4@SiO_2@*m*LDH350) also exhibited similar pH and ionic strength dependent behaviors as mentioned above, implying the same adsorption mechanisms for all MgAl-LDH composites.

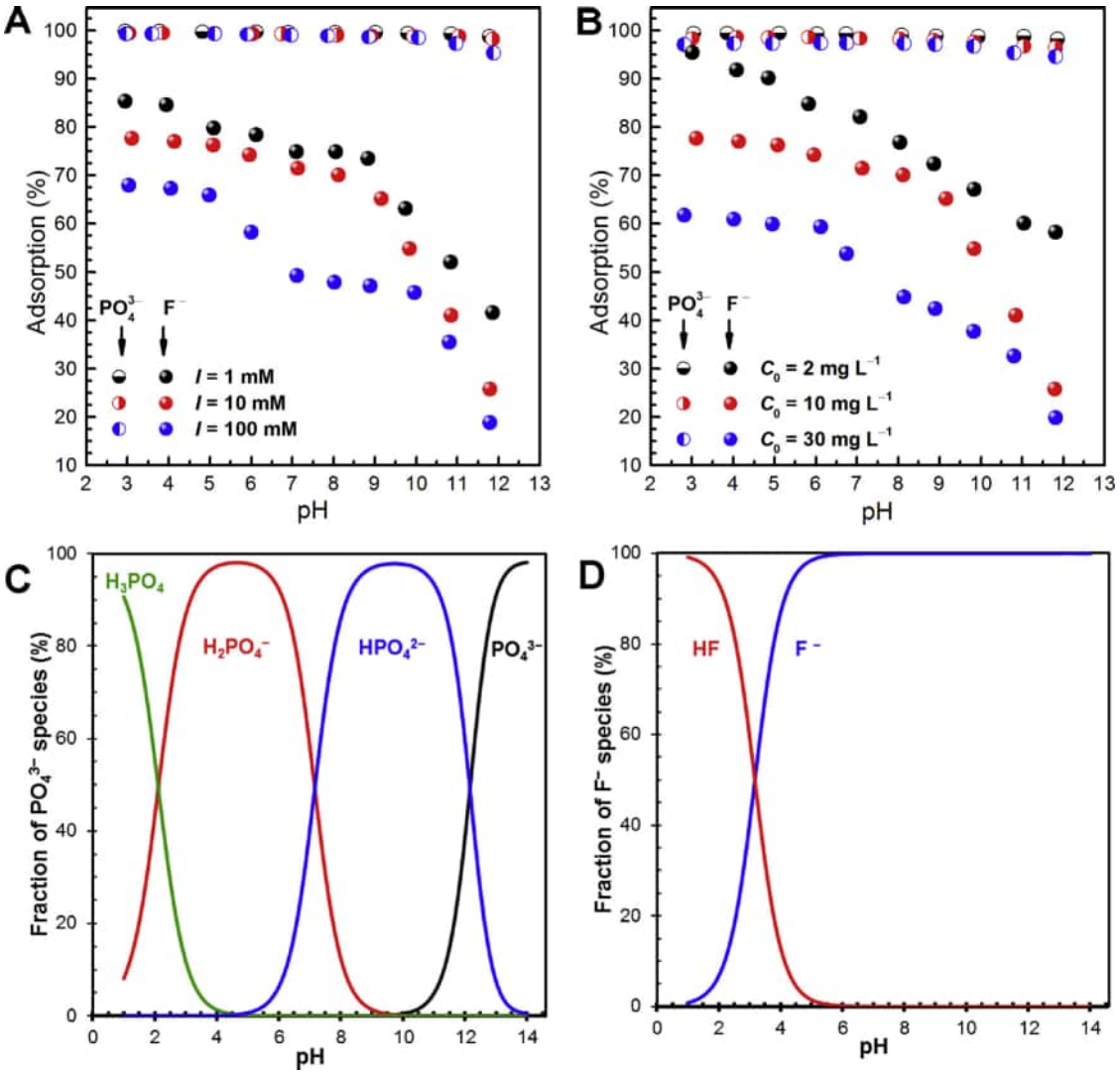

Fig. 4. (A) Effects of pH and ionic strength (I) on phosphate (PO_4^{3-}) and fluoride (F^-) adsorption on Fe_3O_4@$m$$SiO_2$@$m$LDH350, adsorbate$_{initial}$ = 10 mg L^{-1} (adsorbate = PO_4^{3-} or F^-), sorbent dosage = 1 g L^{-1}, T = 25 °C; (B) Effects of pH and initial adsorbate concentrations (C_0) on PO_4^{3-} and F^- adsorption on Fe_3O_4@$m$$SiO_2$@$m$LDH350, I = 10 mM $NaNO_3$, sorbent dosage = 1 g L^{-1}, T = 25 °C; Aqueous speciation of (C) PO_4^{3-} and (D) F^- as a function of pH.

3.4. Effects of pH and initial adsorbate concentrations on P and F adsorption

Likewise, effects of pH and initial adsorbate concentrations (C_0) on phosphate and fluoride adsorption were studied from pH 3 to 12 with initial adsorbate (i.e., PO_4^{3-} or F^-) concentrations of 2 mg L^{-1}, 10 mg L^{-1}, and 30 mg L^{-1}, respectively. The results were given in Fig. 4B and S5. Obviously, the phosphate adsorption efficiencies displayed almost independent upon both the pH values and the initial phosphate concentrations (C_0) at pH < pH_{PZC}, which implies that most phosphates were bound as inner-sphere complexes rather than as the intercalated anions (Goldberg, 2014). Due to the increasing competition from OH^- and the increasing Coulomb repulsion at pH above pH_{PZC}, the adsorption efficiencies were expected to decrease slightly with an increase in the initial phosphate concentrations from 2 mg L^{-1} to 30 mg L^{-1}. This observation is in good consonance with the above results of pH and ionic strength effects, confirming that inner-sphere complexation played a crucial role in phosphate adsorption. Nevertheless, Das et al. (2006) have investigated the effect of initial phosphate concentration on Adsorption% of phosphate by calcined MgAl-LDHs. It was found that Adsorption% of phosphate were apparently dependent upon both pH values and the initial phosphate concentration and that Adsorption% of phosphate decreased significantly with increasing C_0 from 30 mg L^{-1} to 70 mg L^{-1}. This is quite different from our data as described above. The reasons would probably be attributed to the differences in the phase compositions as well as the microstructures of the MgAl-LDH sorbents, which in turn resulted in different adsorption behaviors of phosphate.

On the other hand, F^- adsorption on Fe_3O_4@$m$$SiO_2$@$m$LDH350 has shown similar pH- and C_0-dependent behaviors as observed above. This further confirmed that F^- adsorption on the MgAl-LDH composites was dominated by the anionic exchange process. In the cases of phosphate and fluoride adsorption on the other two MgAl-LDH composites (i.e., Fe_3O_4@SiO_2@LDH350, and Fe_3O_4@SiO_2@mLDH350), both phosphate and fluoride have shown as similar adsorption behaviors as observed for Fe_3O_4@$m$$SiO_2$@$m$LDH350 (Fig. S5). This is expected because of the high degree of similarity in phase compositions and microstructures of all the MgAl-LDH composites.

3.5. Adsorption isotherms and mechanism

Fig. 5 displays the adsorption isotherms of phosphate and fluoride on the mesoporous MgAl-LDH composites. The experimental data were fitted with both the Langmuir (solid lines) and the Freundlich (dashed

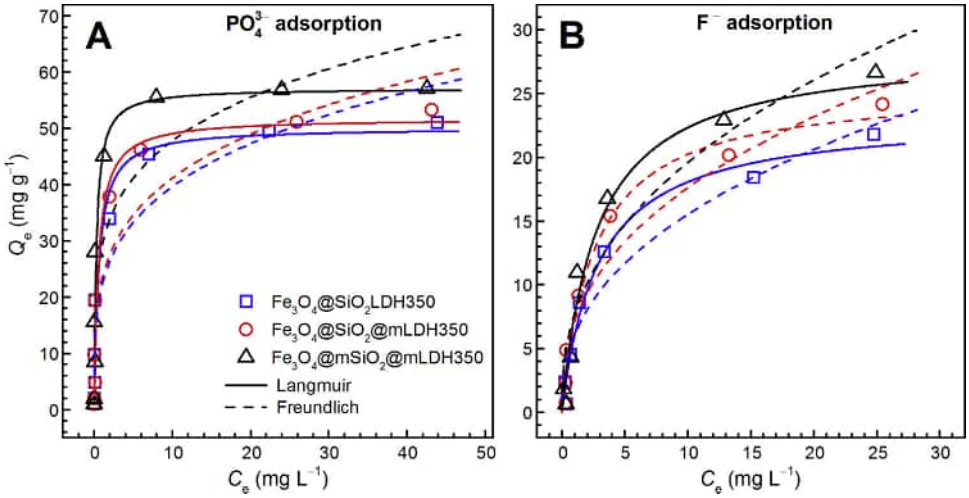

Fig. 5. Adsorption isotherms of (A) phosphate (PO_4^{3-}) and (B) fluoride (F^-) on three MgAl-LDH composites (sorbent dosage = 1 g L^{-1}, T = 25 °C, contact time = 24 h).

lines) models by using the nonlinear algorithms (Eqs. (3) and (4)) as given below.

Langmuir Model:

$$Q_e = \frac{k_L Q_m C_e}{1 + k_L C_e} \tag{3}$$

Freundlich Model:

$$Q_e = k_F C_e^{1/n} \tag{4}$$

where Q_e is the adsorption capacity in the equilibrium state (mg g^{-1}), Q_m is the theoretical maximum adsorption capacity, C_e is the equilibrium concentration of the target adsorbate (mg L^{-1}), k_L is the Langmuir constant related to free energy of adsorption (L mg^{-1}), k_F (in L g^{-1}) and n are empirical constants associated with the Freundlich model. The fitting parameters were calculated by Origin 9.0 (64-bit version, OriginLab Co.) and are tabulated in Table 1. It was found that the adsorption capacities (Q_e) increased with increasing equilibrium concentrations of either phosphate or fluoride (C_e), and reached or was approaching a plateau which represents the maximum adsorption capacity of the MgAl-LDH composites for the target adsorbate, e.g., phosphate or fluoride.

A comparison of the correlation coefficients (R^2) (Table 1) indicates that all the correlation coefficients of the Langmuir model are greater than those of Freundlich model, suggesting that the Langmuir model is better than the Freundlich model to fit the adsorption data. The maximum adsorption capacities of phosphate calculated by the Langmuir equation (Eq. (3)) are 50.07 mg g^{-1}, 51.70 mg g^{-1}, and 57.07 mg g^{-1} for Fe_3O_4@SiO_2@LDH350, Fe_3O_4@SiO_2@*m*LDH350, and Fe_3O_4@*m*SiO_2@*m*LDH350, respectively. Whereas, these MgAl-LDH composites have maximum adsorption capacities of 23.28 mg g^{-1}, 25.47 mg g^{-1}, and 28.52 mg g^{-1} for fluoride, respectively, much lower than those for phosphate. It is noteworthy that the sample with dual mesoporous shells, i.e., Fe_3O_4@*m*SiO_2@*m*LDH350 has the highest Q_m values for both phosphate and fluoride among all MgAl-LDH composites, although it does not have the largest BET specific surface area. This indicates that besides specific surface area, other parameters such as the pore size distribution (see Fig. 1D), and/or the available adsorption site density may contribute more to the adsorption capacity of these MgAl-LDH composites (Goldberg, 2014).

For comparison, the Q_m values of both phosphate and fluoride of other LDHs-type sorbents are summarized in Tables 2 and 3. In the case of phosphate (Table 2), the highest adsorption of 57.07 mg g^{-1} was obtained on Fe_3O_4@*m*SiO_2@*m*LDH350 as compared with other LDHs-type sorbents such as MgAl-CLDHs (44.0 mg g^{-1}) (Das et al., 2006), ZnAl-CLDHs (54.1 mg g^{-1}) (Zhou et al., 2011), MgFeZr-LDHs (30.0 mg g^{-1}) (Mandel et al., 2013), Fe_3O_4@ZnAl-LDHs (36.9 mg g^{-1}) (Yan et al., 2015), MgAlZr-LDHs (30.0 mg g^{-1}) (Chitrakar et al., 2007), and ZnAl-CLDHs (41.26 mg g^{-1}) (Cheng et al., 2010). Kannan et al. have reported a ZnAlZr-LDH sorbent with a phosphate adsorption capacity as high as 148.0 mg g^{-1} (Koilraj and Kannan, 2010). However, the higher capacity as compared to the above LDH sorbents was primarily attributed to the formation of surface precipitation, i.e., the hopeite mineral ($Zn_3(PO_4)_2{\cdot}4H_2O$), leading to a poor recycling performance for phosphate adsorption. In the case of fluoride (Table 3), all the MgAl-LDH composites have higher adsorption capacity maxima than other LDHs-type sorbents except for MgAl-CLDHs (80.0 mg g^{-1}) (Lv et al., 2006). Adsorption density (Γ) is also employed as an indicator of adsorption performance. As shown in Tables 2 and 3, the Γ values of all core/shell/shell MgAl-LDH composites for both phosphate and fluoride are high and comparable to that of the best LDHs sorbent (e.g., 0.33 mg m^{-2} for MgAl-CLDHs vs. 0.32 mg m^{-2} for Fe_3O_4@SiO_2@LDH350). Moreover, it is evident that all the n values of Freundlich constant are greater than 2 (Table 1), implying that both phosphate and fluoride adsorption on all MgAl-LDH composites are a favorable process

Table 1
Langmuir and Freundlich models fitting parameters for PO_4^{3-} and F^- adsorption on the core/shell/shell MgAl-LDH composites.

Adsorbate	Sorbent	Langmuir model			Freundlich model		
		Q_m (mg g^{-1})	K_L (L mg^{-1})	R^2	K_F (mg^{1-n} L^n) g^{-1}	n	R^2
PO_4^{3-}	Fe_3O_4@SiO_2@LDH350	50.07	1.72	0.951	22.05	3.92	0.884
	Fe_3O_4@SiO_2@mLDH350	51.70	1.83	0.961	23.07	3.98	0.873
	Fe_3O_4@mSiO_2@mLDH350	57.07	3.44	0.936	29.04	4.63	0.821
F^-	Fe_3O_4@SiO_2@LDH350	23.28	0.35	0.981	6.03	2.44	0.942
	Fe_3O_4@SiO_2@*m*LDH350	25.47	0.39	0.978	6.29	2.53	0.937
	Fe_3O_4@*m*SiO_2@*m*LDH350	28.52	0.36	0.971	7.61	2.43	0.915

Table 2
Caparison of the P adsorption capacity maxima on the core/shell/shell MgAl-LDH composites with other LDHs-type sorbents.

LDHs	pH	BET ($m^2 g^{-1}$)	Q_m ($mg\ g^{-1}$)	Γ ($mg\ m^{-2}$)	Refs
MgAl-CLDHs	6	210	44.0	0.21	(Das et al., 2006)
ZnAl-CLDHs	7	232	54.1	0.23	(Zhou et al., 2011)
MgFeZr-LDHs	7-8	100	30.0	0.30	(Mandel et al., 2013)
Fe_3O_4@ZnAl-LDHs	7	133	36.9	0.28	(Yan et al., 2015)
MgAlZr-LDHs	8.7	139	30.0	0.22	(Chitrakar et al., 2007)
ZnAl-CLDHs	7	81.2	41.26	0.51	(Cheng et al., 2010)
ZnAlZr-LDHs	7	78	148.0	1.90	(Koilraj and Kannan, 2010)
Fe_3O_4@SiO_2@LDH350	7.5	73	50.07	0.69	This study
Fe_3O_4@SiO_2@*m*LDH350	7.5	168	51.70	0.31	This study
Fe_3O_4@*m*SiO_2@*m*LDH350	7.5	137	57.07	0.42	This study

(Wen et al., 2013). It is, therefore, believed that these mesoporous MgAl-LDH composites with such high adsorption capacities for both phosphate and fluoride are expected to have the potential for application in practical wastewater remediation.

To further study the adsorption mechanism, both pristine and exhausted Fe_3O_4@*m*SiO_2@*m*LDH350 were employed to perform the XRD, FTIR, and XPS analyses and the results are present in Fig. 6. Fig. 6A shows the XRD patterns of Fe_3O_4@*m*SiO_2@*m*LDH350 before and after phosphate or fluoride adsorption. Obviously, the reflections attributable to the layered MgAl-LDHs remained after phosphate or fluoride adsorption, implying that Fe_3O_4@*m*SiO_2@*m*LDH350 is robust enough. However, the intensities decreased apparently after adsorption of either phosphate or fluoride, indicating that no reconstruction of the calcinated layered MgAl-LDH occurred during the adsorption process (Ji et al., 2017). and that the adsorption of fluoride exhibited an apparent negative effect on the crystallinity of Fe_3O_4@*m*SiO_2@*m*LDH350. The *d* spacing of (003) reflection varied from 8.09 Å to 7.86 Å and 7.34 Å respectively after adsorption of phosphate and fluoride, which is in good agreement to previous studies (Cai et al., 2012). As shown in the FTIR spectra (Fig. 6B), a weak band at 1055 cm^{-1} assignable to the asymmetrical stretching vibration of PO_4^{3-} appeared after phosphate adsorption, demonstrating that phosphate was bound. Nevertheless, in the case of fluoride adsorption, no band attributed to fluoride was observed due to the infrared inactivity of fluoride compounds (e.g., there are no other bands for sodium fluoride (NaF) except for the surface hydroxyl band of absorbed water, data not shown). Besides, a weak carbonate band at 1361 cm^{-1} appeared after adsorption of either fluoride or phosphate, which was apparently derived from the anionic exchange of interlayer NO_3^- with the aqueous CO_3^{2-} originated from the atmospheric carbon dioxide.

The full-range XPS spectra also confirmed that either phosphate or fluoride has been adsorbed on Fe_3O_4@*m*SiO_2@*m*LDH350 (Fig. 6C). The O 1s spectrum of pristine Fe_3O_4@*m*SiO_2@*m*LDH350 consists of four peaks (Fig. 6D), which could be assigned to oxygen atoms in M–O (M = Mg or Al, 529.8 eV), OH (531.4 eV), N-O(531.8 eV) in NO_3^- and H_2O, CO_3^{2-} (533.6 eV), respectively (Circu et al., 2016; Xie et al., 2017). After phosphate adsorption, the existence of phosphate is confirmed by the P 2p XPS spectrum (Fig. S6), which can be further differentiated into P $2p_{1/2}$ and P $2p_{3/2}$ peaks. The best fit of O 1s spectrum was obtained with four components corresponding to oxygen atoms in M–O (529.7 eV), M–O-P, P = O (531.0 eV), POH, NO_3^- (532.1 eV), and H_2O, CO_3^{2-} (533.2 eV). The N 1s spectrum shifted (Fig. S6) from 407.8 eV to 406.4 eV with a dramatic decrease in intensity, implying the occurring of anionic exchange between the interlayer nitrate and phosphate in solution. In the case of fluoride, the F 1s XPS spectrum (Fig. S6) also demonstrates fluoride was successfully bound. Likewise, the best fit of O 1s spectrum was achieved with four components ascribed to oxygen atoms in M–O (529.7 eV), OH (531.2 eV), NO_3^- (532.3 eV), and H_2O, CO_3^{2-} (532.9 eV). The N 1s spectrum also shifted from 407.8 eV to 406.8 eV with a strong intensity decrease, indicating that fluoride was adsorbed by a manner of anionic exchange.

According to the above results, a possible mechanism for phosphate and fluoride adsorption on the MgAl-LDH composites was proposed, which involves in i) anionic exchange between the interlayered nitrate and the anions in solution (i.e., phosphate and fluoride), and ii) surface complexation of anions with the surface metal hydroxyls (> M–OH) of the MgAl-LDH composites. In the case of surface complexation, phosphate is likely to be bound as bidentate binuclear inner-sphere complexes (Li et al., 2013), whereas fluoride is probably retained by outer-sphere complexation. These reactions can be formulated as follows,

Anionic exchange:

$$> M\text{–}OH_2^+/NO_3^- + F^- \leftrightarrow > M\text{–}OH_2^+/F^- + NO_3^- \quad (5)$$

$$> M\text{–}OH_2^+/NO_3^- + H_2PO_4^- \leftrightarrow > M\text{–}OH_2^+/H_2PO_4^- + NO_3^- \quad (6)$$

Surface complexation:

$$> M\text{–}OH + F^- + H^+ \leftrightarrow > M\text{–}OH_2^+/F^- \quad (7)$$

$$2(> M\text{–}OH) + PO_4^{3-} + 2H^+ \leftrightarrow > M_2PO_4^- + 2H_2O \quad (8)$$

$$2(> M\text{–}OH) + PO_4^{3-} + 3H^+ \leftrightarrow > M_2PO_4H + 2H_2O \quad (9)$$

3.6. Desorption and recycling performance

Two mesoporous MgAl-LDH composites, i.e., Fe_3O_4@SiO_2@*m*LDH350 and Fe_3O_4@*m*SiO_2@*m*LDH350 were chosen as sorbents to explore their recycling performance, and the results are given in Fig. 7. In the case of phosphate, the adsorption efficiency on Fe_3O_4@SiO_2@

Table 3
Caparison of the F adsorption capacity maxima on the core/shell/shell MgAl-LDH composites with other LDHs-type sorbents.

LDHs	pH	BET ($m^2 g^{-1}$)	Q_m ($mg\ g^{-1}$)	Γ ($mg\ m^{-2}$)	Refs
MgAl LDHs	7	413	1.65	0.004	(Wang et al., 2007)
MgAl-CLDHs	6	240	80.0	0.33	(Lv et al., 2006)
MgAl-CLDHs	6	–	1.94	–	(Cai et al., 2012)
Fe_3O_4@SiO_2@LDH350	7.5	73	23.28	0.32	This study
Fe_3O_4@SiO_2@*m*LDH350	7.5	168	25.47	0.15	This study
Fe_3O_4@*m*SiO_2@*m*LDH350	7.5	137	28.52	0.21	This study

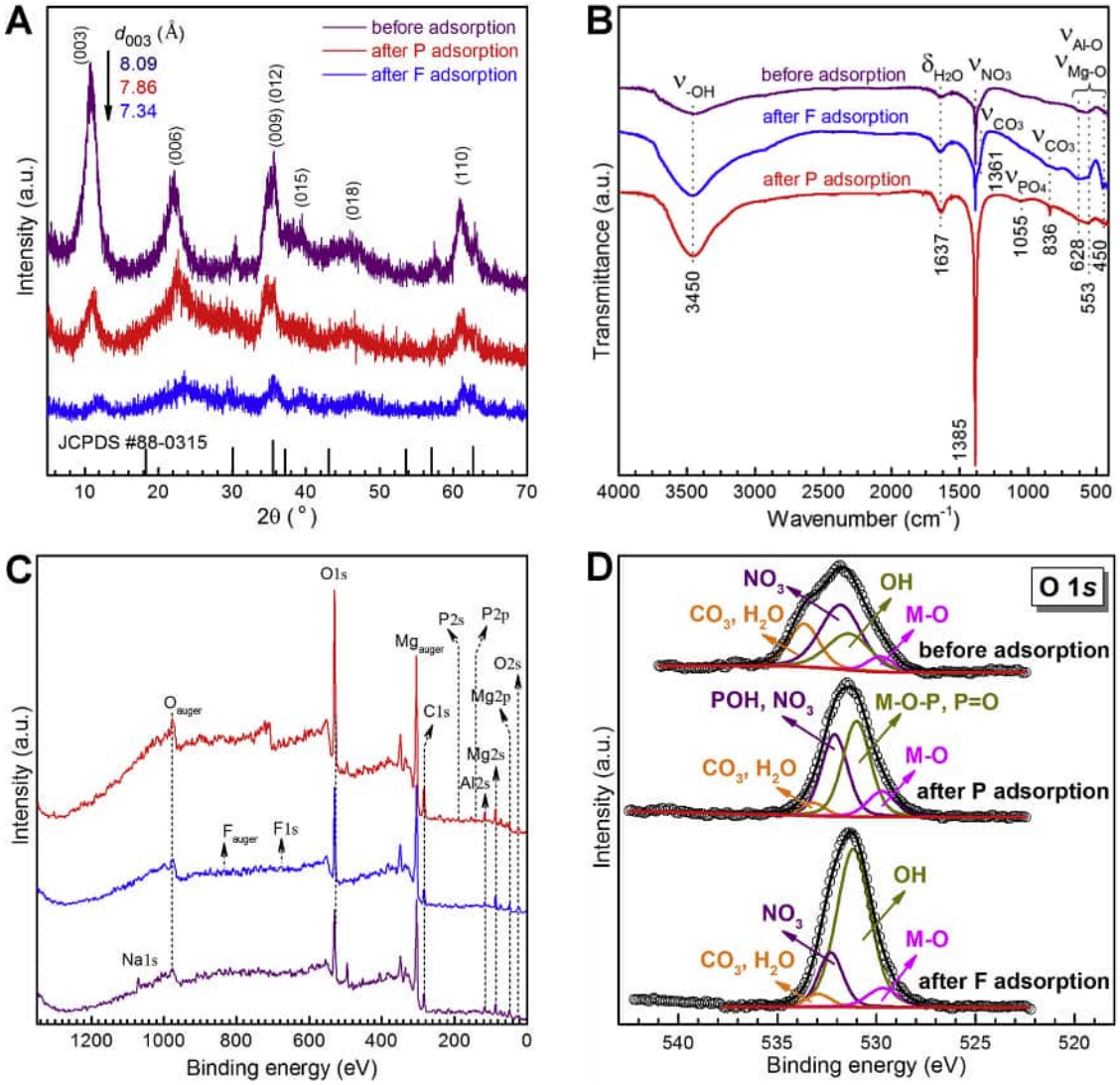

Fig. 6. (A) XRD patterns, (B) FTIR spectra, (C) survey scans of XPS spectra, (D) high-resolution scans of O1 s peaks of Fe_3O_4@mSiO_2@mLDH350 before and after adsorption of PO_4^{3-} and F^-.

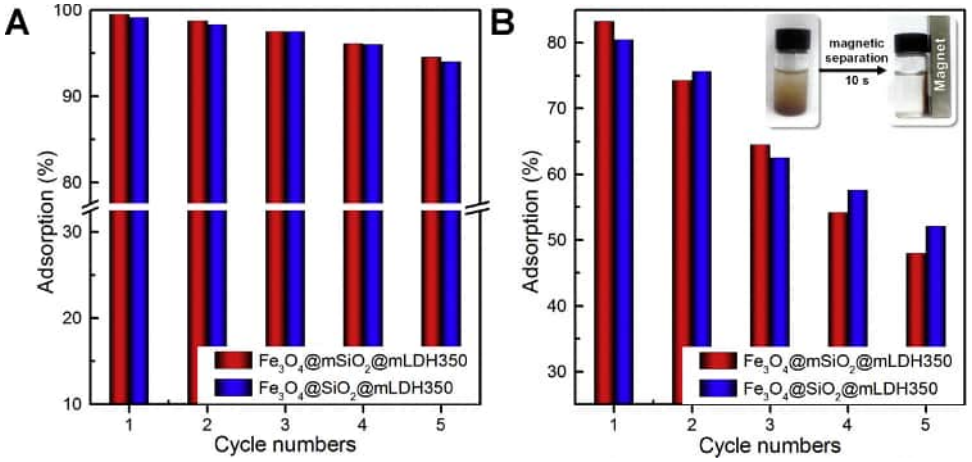

Fig. 7. Recycling performance of two mesoporous MgAl-LDH composites for adsorption of (A) PO_4^{3-} and (B) F^- during 5-time recycling, the inset in panel B is the digital photograph of magnetic separation of the sorbent suspensions in 10 s (C_0 = 10 mg L^{-1}, sorbent dose = 1 g L^{-1}, T = 25 °C, contact time = 24 h).

*m*LDH350 decreased from 99.1% to 94.0% after five-time recycling, while the adsorption efficiency declined from 99.5% to 94.5% for Fe_3O_4@*m*SiO_2@*m*LDH350, indicating superb recycling performance for both MgAl-LDH composites toward phosphate, which endows them with a potential utilization as slow-release phosphate fertilizer (Benicio et al., 2017; Everaert et al., 2016). On the other hand, the adsorption efficiencies of fluoride decreased respectively from 80.0%, and 83.2% to 52.1%, and 47.9% for the two MgAl-LDH composites. In order to improve and optimize the regeneration performance of magnetic adsorbent, Drenkova-Tuhtan et al. employed a stepwise adsorption-desorption regeneration, of which the adsorption and desorption time of the first 10 cycles were set to 1 h (Drenkova-Tuhtan et al., 2017). A preliminary adsorption kinetic experiment using Fe_3O_4@*m*SiO_2@*m*LDH350 as the sorbent indicates that Adsorption% of fluoride reaches at 84.1% of its maxima, while Adsorption% of phosphate achieves to 78.9% of its maxima after 1 h adsorption (Fig. S7). Therefore, further regeneration experiments in a manner of 1 h adsorption, 10 s magnetic separation, and 1 h desorption and repetition the above process for 10 cycles were performed for fluoride using Fe_3O_4@*m*SiO_2@*m*LDH350 as the sorbent. In the case of phosphate, similar regeneration experiments with 2 h adsorption followed by 10 s magnetic separation, 2 h desorption and then repetition were also conducted. The recycling results are given in Fig. S8. Apparently, the recovery of either phosphate or fluoride by Fe_3O_4@*m*SiO_2@*m*LDH350 in such quick manners is slightly less than those in the manner of 24 h adsorption plus 24 h desorption (*cf.* Fig. 7 and S8). Note that the recovery of phosphate by Fe_3O_4@*m*SiO_2@*m*LDH350 was approximately 90% for the first cycle and gradually dropped to 68.5% for the tenth cycle, whereas the recovery of fluoride decreased rapidly from 81.2% for the first cycle to 27.1% for the tenth cycle (Fig. S8). As mentioned above, fluoride has shown an adverse effect on the crystallinity of MgAl-LDH composites (Fig. 6A). This could probably result in the partial collapse of the mesoporous structure of MgAl-LDH composites, which consequently led to such fair recycling performance for fluoride. The drop in recycling performance of phophate adsorption seems also to partly attribute to the recessioin of the outermost mesoprous LDH layers during the regeneration process (Ji et al., 2017). Future experiments on the improvement of the recycling performance of MgAl-LDH composites towards fluoride and phosphate uptake should center around enhancing the stability of mesostructured MgAl-LDH and increasing the adsorption capacity by introduction of some rare earth species (e.g., La and Zr) into the MgAl-LDH layers (Jing et al., 2012). Nevertheless, from a practical point of view, both MgAl-LDH composites with high adsorption capacities, and features of easy to separate from solution by an external magnet (inset of Fig. 7B) are expected to use as an alternative to commercial sorbents for phosphate and fluoride removal from aqueous solutions.

4. Conclusions

In summary, core/shell/shell hierarchical structured mesoporous MgAl-LDH composites were prepared. The mesoporous MgAl-LDH composites exhibit large surface areas and well-defined mesopore distributions, which endows them much higher adsorption capacities toward both phosphate and fluoride as compared with other LDH-type materials. The corresponding adsorption mechanisms involve both anionic exchange and surface complexation. Moreover, the presence of the magnetite (Fe_3O_4) core allows them to be easily separated by an external magnetic field, facilitating their recycling and reuse. Due to the good reusability, these mesoporous core/shell/shell MgAl-LDH composites can be potentially used as sorbents for removal or recovery of phosphate and fluoride from water.

Author contributions section

F.L. designed research; F.L., J.J., Z.S., H.J., M. Y., Y.Y. performed research; F.L., and J.J. analyzed data; and F.L. wrote the paper.

Acknowledgments

The work was supported by Postgraduate Research & Practice Innovation Program of Jiangsu Province (SJCX17-0261), NSFC (51002080, 41501197), SPITP (201610300273), Top-notch Academic Programs Project of Jiangsu Higher Education Institutions (PPZY2015C222), and the Priority Academic Program Development of Jiangsu Higher Education Institutions (PAPD).

Appendix B. Supplementary data

Supplementary material related to this article can be found, in the online version, at doi:https://doi.org/10.1016/j.jhazmat.2019.121734.

References

Ayoob, S., Gupta, A.K., 2006. Fluoride in drinking water: a review on the status and stress effects. Crit. Rev. Env. Sci. Technol. 36, 433–487.
Benicio, L.P.F., Constantino, V.R.L., Pinto, F.G., Vergutz, L., Tronto, J., da Costa, L.M., 2017. Layered double hydroxides: new technology in phosphate fertilizers based on nanostructured materials. ACS Sustain. Chem. Eng. 5, 399–409.
Bhatnagar, A., Kumar, E., Sillanpaa, M., 2011. Fluoride removal from water by adsorption-a review. Chem. Eng. J. 171, 811–840.
Cai, P., Zheng, H., Wang, C., Ma, H.W., Hu, J.C., Pu, Y.B., Liang, P., 2012. Competitive adsorption characteristics of fluoride and phosphate on calcined Mg-Al-CO_3 layered double hydroxides. J. Hazard. Mater. 213, 100–108.
Cai, J.G., Zhang, Y.Y., Pan, B.C., Zhang, W.M., Lv, L., Zhang, Q.X., 2016. Efficient defluoridation of water using reusable nanocrystalline layered double hydroxides impregnated polystyrene anion exchanger. Water Res. 102, 109–116.
Camargo, J.A., 2003. Fluoride toxicity to aquatic organisms: a review. Chemosphere 50, 251–264.
Cheng, X., Huang, X.R., Wang, X.Z., Sun, Z., 2010. Influence of calcination on the adsorptive removal of phosphate by Zn-Al layered double hydroxides from excess sludge liquor. J. Hazard. Mater. 177, 516–523.
Chitrakar, R., Tezuka, S., Sonoda, A., Sakane, K., Ooi, K., Hirotsu, T., 2007. Synthesis and phosphate uptake behavior of Zr^{4+} incorporated MgAl-layered double hydroxides. J. Colloid Interface Sci. 313, 53–63.
Chubar, N., Gilmour, R., Gerda, V., Micusik, M., Omastova, M., Heister, K., Man, P., Fraissard, J., Zaitsev, V., 2017. Layered double hydroxides as the next generation inorganic anion exchangers: synthetic methods versus applicability. Adv. Colloid Interface Sci. 245, 62–80.
Circu, M., Nan, A., Borodi, G., Liebscher, J., Turcu, R., 2016. Refinement of magnetite nanoparticles by coating with organic stabilizers. NanomaterialsBasel 6, 228.
Correll, D.L., 1998. The role of phosphorus in the eutrophication of receiving waters: a review. J. Environ. Qual. 27, 261–266.
Das, J., Patra, B.S., Baliarsingh, N., Parida, K.M., 2006. Adsorption of phosphate by layered double hydroxides in aqueous solutions. Appl. Clay Sci. 32, 252–260.
Delgado, R.R., De Pauli, C.P., Carraseo, C.B., Avena, M.J., 2008. Influence of M-II/M-III ratio in surface-charging behavior of Zn-Al layered double hydroxides. Appl. Clay Sci. 40, 27–37.
Ding, H., Zhao, Y.L., Duan, Q.L., Wang, J.W., Zhang, K., Ding, G.Y., Xie, X.M., Ding, C.M., 2017. Efficient removal of phosphate from aqueous solution using novel magnetic nanocomposites with Fe_3O_4@SiO_2 core and mesoporous CeO_2 shell. J. Rare Earth. 35, 984–994.
Drenkova-Tuhtan, A., Mandel, K., Paulus, A., Meyer, C., Hutter, F., Gellermann, C., Sextl, G., Franzreb, M., Steinmetz, H., 2013. Phosphate recovery from wastewater using engineered superparamagnetic particles modified with layered double hydroxide ion exchangers. Water Res. 47, 5670–5677.
Drenkova-Tuhtan, A., Schneider, M., Franzreb, M., Meyer, C., Gellermann, C., Sextl, G., Mandel, K., Steinmetz, H., 2017. Pilot-scale removal and recovery of dissolved phosphate from secondary wastewater effluents with reusable ZnFeZr adsorbent @ Fe_3O_4/SiO_2 particles with magnetic harvesting. Water Res. 109, 77–87.
Eliasson, J., 2015. The rising pressure of global water shortages. Nature 517, 6.
Everaert, M., Warrinnier, R., Baken, S., Gustafsson, J.P., De Vos, D., Smolders, E., 2016. Phosphate-exchanged Mg-Al layered double hydroxides: a new slow release phosphate fertilizer. ACS Sustain. Chem. Eng. 4, 4280–4287.
Goh, K.H., Lim, T.T., Dong, Z.L., 2008. Application of layered double hydroxides for removal of oxyanions: a review. Water Res. 42, 1343–1368.
Goldberg, S., 2014. Application of surface complexation models to anion adsorption by natural materials. Environ. Toxicol. Chem. 33, 2172–2180.
Gunawan, P., Xu, R., 2009. Direct assembly of anisotropic layered double hydroxide (LDH) nanocrystals on spherical template for fabrication of Drug-LDH hollow nanospheres. Chem. Mater. 21, 781–783.
Huang, Q.J., Liao, M.C., Zeng, H.Y., Zhang, W., Zhang, Z.Q., Liu, X.J., Li, H., 2014. Effects of surface pretreatment on structure and release performances of Mg-Al hydrotalcites. Chinese J. Inorg. Chem. 30, 1542–1548.
Ji, H.S., Wu, W.H., Li, F.H., Yu, X.X., Fu, J.J., Jia, L.Y., 2017. Enhanced adsorption of bromate from aqueous solutions on ordered mesoporous Mg-Al layered double hydroxides (LDHs). J. Hazard. Mater. 334, 212–222.
Jia, Z.Q., Hao, S., Lu, X.Y., 2018. Exfoliated Mg-Al-Fe layered double hydroxides/polyether sulfone mixed matrix membranes for adsorption of phosphate and fluoride from

aqueous solutions. J. Environ. Sci.-China 70, 63–73.
Jing, C.Y., Cui, J.L., Huang, Y.Y., Li, A.G., 2012. Fabrication, characterization, and application of a composite adsorbent for simultaneous removal of arsenic and fluoride. ACS Appl. Mater. Interfaces 4, 714–720.
Kameda, T., Oba, J., Yoshioka, T., 2017. Removal of boron and fluoride in wastewater using Mg-Al layered double hydroxide and Mg-Al oxide. J. Environ. Manage. 188, 58–63.
Koilraj, P., Kannan, S., 2010. Phosphate uptake behavior of ZnAlZr ternary layered double hydroxides through surface precipitation. J. Colloid Interface Sci. 341, 289–297.
Li, F.H., Wu, W.H., Li, R.Y., Fu, X.R., 2016. Adsorption of phosphate by acid-modified fly ash and palygorskite in aqueous solution: experimental and modeling. Appl. Clay Sci. 132, 343–352.
Li, F.H., Fu, J.J., Jin, J., Wang, S.L., Liu, Y.Y., Yang, M., Fu, X.R., 2019. Evaporation-induced self-assembly (EISA) synthesized mesoporous bimetallic oxides (MBOs) enabling enhanced co-uptake of arsenate and fluoride from water. J. Chem. Technol. Biotechnol. 94, 879–891.
Li, W., Pierre-Louis, A.M., Kwon, K.D., Kubicki, J.D., Strongin, D.R., Phillips, B.L., 2013. Molecular level investigations of phosphate sorption on corundum (alpha-Al2O3) by P-31 solid state NMR, ATR-FTIR and quantum chemical calculation. Geochim. Cosmochim. Acta 107, 252–266.
Loganathan, P., Vigneswaran, S., Kandasamy, J., Bolan, N.S., 2014. Removal and recovery of phosphate from water using sorption. Crit. Rev. Env. Sci. Technol. 44, 847–907.
Lv, L., He, J., Wei, M., Evans, D.G., Duan, X., 2006. Factors influencing the removal of fluoride from aqueous solution by calcined Mg-Al-CO_3 layered double hydroxides. J. Hazard. Mater. 133, 119–128.
Mandel, K., Drenkova-Tuhtan, A., Hutter, F., Gellermann, C., Steinmetz, H., Sextl, G., 2013. Layered double hydroxide ion exchangers on superparamagnetic microparticles for recovery of phosphate from waste water. J. Mater. Chem. A Mater. Energy Sustain. 1, 1840–1848.
Morse, G.K., Brett, S.W., Guy, J.A., Lester, J.N., 1998. Review: Phosphorus removal and recovery technologies. Sci. Total Environ. 212, 69–81.
Park, J.Y., Kim, J.H., 2011. Characterization of adsorbed arsenate on amorphous and nano crystalline MgFe-layered double hydroxides. J. Nanopart. Res. 13, 887–894.
Seftel, E.M., Ciocarlan, R.G., Michielsen, B., Meynen, V., Mullens, S., Cool, P., 2018. Insights into phosphate adsorption behavior on structurally modified ZnAl layered double hydroxides. Appl. Clay Sci. 165, 234–246.
Shao, M.F., Ning, F.Y., Zhao, J.W., Wei, M., Evans, D.G., Duan, X., 2012. Preparation of Fe_3O_4@SiO_2@Layered double hydroxide core-shell microspheres for magnetic separation of proteins. J. Am. Chem. Soc. 134, 1071–1077.
Sharpley, A.N., Chapra, S.C., Wedepohl, R., Sims, J.T., Daniel, T.C., Reddy, K.R., 1994. Managing agricultural phosphorus for protection of surface waters - issues and options. J. Environ. Qual. 23, 437–451.
Thommes, M., Kaneko, K., Neimark, A.V., Olivier, J.P., Rodriguez-Reinoso, F., Rouquerol, J., Sing, K.S.W., 2015. Physisorption of gases, with special reference to the evaluation of surface area and pore size distribution (IUPAC Technical Report). Pure Appl. Chem. 87, 1051–1069.
Ulibarri, M.A., Hermosin, M.C., 2001. Layered double hydroxides in water decontamination. In: Rives, V. (Ed.), Layered Double Hydroxides: Present and Future. Nova Science Publishers, New York, pp. 288.
Wang, H.T., Chen, J., Cai, Y.F., Ji, J.F., Lin, L.W., Teng, H.H., 2007. Defluoridation of drinking water by Mg/Al hydrotalcite-like compounds and their calcined products. Appl. Clay Sci. 35, 59–66.
Wen, T., Wu, X.L., Tan, X.L., Wang, X.K., Xu, A.W., 2013. One-pot synthesis of water-swellable Mg-Al layered double hydroxides and graphene oxide nanocomposites for efficient removal of As(V) from aqueous solutions. ACS Appl. Mater. Interfaces 5, 3304–3311.
Xie, Q.Y., Li, Y., Lv, Z.L., Zhou, H., Yang, X.J., Chen, J., Guo, H., 2017. Effective adsorption and removal of phosphate from aqueous solutions and eutrophic water by Fe-based MOFs of MIL-101. Sci. Rep. 7, 3316.
Yan, H.L., Chen, Q.W., Liu, J.H., Feng, Y., Shih, K.M., 2018. Phosphorus recovery through adsorption by layered double hydroxide nano-composites and transfer into a struvite-like fertilizer. Water Res. 145, 721–730.
Yan, L.G., Yang, K., Shan, R.R., Yan, T., Wei, J., Yu, S.J., Yu, H.Q., Du, B., 2015. Kinetic, isotherm and thermodynamic investigations of phosphate adsorption onto core-shell Fe_3O_4@LDHs composites with easy magnetic separation assistance. J. Colloid Interface Sci. 448, 508–516.
Zhang, X.F., Wang, J., Li, R.M., Dai, Q.H., Gao, R., Liu, Q., Zhang, M.L., 2013. Preparation of Fe_3O_4@C@Layered double hydroxide composite for magnetic separation of uranium. Ind. Eng. Chem. Res. 52, 10152–10159.
Zhou, J.B., Yang, S.L., Yu, J.G., Shu, Z., 2011. Novel hollow microspheres of hierarchical zinc-aluminum layered double hydroxides and their enhanced adsorption capacity for phosphate in water. J. Hazard. Mater. 192, 1114–1121.